X-ray Spectroscopy of Nitric Oxide Binding to Iron in Inactive Nitrile Hydratase and a Synthetic Model Compound

Robert C. Scarrow,*,† Brent S. Strickler,† Jeffrey J. Ellison,‡ Steven C. Shoner,‡ Julie A. Kovacs,*,‡ John G. Cummings,§ and Mark J. Nelson*,§

Contribution from the Department of Chemistry, Haverford College, Haverford, Pennsylvania 19041, Central Research and Development, DuPont, Wilmington, Delaware 19880-0328, and Department of Chemistry, University of Washington, Seattle, Washington 98195

Received September 18, 1997. Revised Manuscript Received July 20, 1998

Abstract: Analysis of the iron K-edge X-ray absorption spectrum (XAS) of the "dark", inactive form of nitrile hydratase (NH_{dk}) from *Rhodococcus* sp. R312 confirms a 1:1 stoichiometry of nitric oxide bound to low-spin iron(III). We also report XAS analyses of four iron complexes of the pentadentate ligands 2,3,13,14-tetramethyl-4,8,12-triaza-3,12-pentadecadiene-2,14-dithiolate (L^{2-}, also denoted as $S_2{}^{Me2}N_3(Pr,Pr)^{2-}$) and 2,12-dimethyl-3,7,11-triaza-2,11-tridecadiene-1,13-dithiolate (L'^{2-}, also denoted as $S_2N_3(Pr,Pr)^{2-}$): five-coordinate $\mathbf{Fe^{II}L'}$ and $\mathbf{FeL}^+$ and low-spin six-coordinate $\mathbf{FeL(N_3)}$ and $\mathbf{FeL(NO)}^+$ (cationic species are PF_6^- salts). The XAS of $\mathbf{FeL(N_3)}$ and $\mathbf{FeL(NO)}^+$ closely mimic the spectra of butyrate-stabilized active nitrile hydratase (NH_{lt}) and NH_{dk}, respectively. The 1s → 3d pre-edge peak is about twice as intense in five-coordinate $\mathbf{FeL}^+$ than for the remaining samples, suggesting that the iron in both NH_{lt} and NH_{dk} is six-coordinate. This peak and other edge features are 1 eV higher in energy for NH_{dk} and $\mathbf{FeL(NO)}^+$, consistent with a $\{FeNO\}^6$ electron count for both the enzyme and the model. Analysis of the EXAFS (including multiple scattering effects) for NH_{dk} and $\mathbf{FeL(NO)}^+$ gives the following identical results: a single NO bound per iron with $r_{FeN} = 1.68 \pm 0.03$ Å and ∠FeNO ≈ 165°. In NH_{dk}, the presence of the NO ligand lengthens at least one of the Fe−S bonds relative to those in NH_{lt}. These data show that synthetic inorganic complexes can be designed to assume iron coordination geometries very similar to those of the iron center in nitrile hydratase and confirm results from EPR spin-trapping experiments (Odaka, M.; Fujii, K.; Hoshino, M.; Noguchi, T.; Tsujimura, M.; Nagashima, S.; Yohda, M.; Nagamune, T.; Inoue, Y.; Endo, I. *J. Am. Chem. Soc.* **1997**, *119*, 3785−3791) that photoactivation of nitrile hydratase includes loss of a single NO ligand from the iron.

Within the past decade, nitrile hydratases have been developed as environmentally benign catalysts for industrial production of acrylamide and specialty chemicals.[1] Nitrile hydratases containing either low-spin iron(III) or cobalt(III) ions have been isolated from several species of bacteria. *Rhodococcus* sp. N-771 and sp. R312 produce iron-containing nitrile hydratases with identical amino acid sequences. A recent crystal structure of *Rhodococcus* sp. R312 NH_{lt}[2] shows three cysteine thiolates and two peptide nitrogen ligands to square pyramidal iron (Figure 1b).[3] Only five ligands are seen in the crystal structure, but the EXAFS-derived bond lengths for NH_{lt} support a six-coordinate iron,[4] and EPR and ENDOR measurements show an additional water or (more likely) hydroxide ligand[5−7] that is not seen in the 2.65 Å resolution structure.

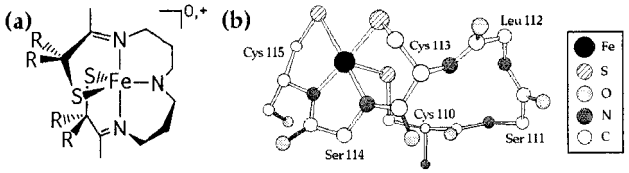

Figure 1. (a) Molecular architecture of $\mathbf{FeL}^+$ (R = CH_3) and $\mathbf{Fe^{II}L'}$ (R = H). $\mathbf{L}^{2-}$ (2,3,13,14-tetramethyl-4,8,12-triaza-3,12-pentadecadiene-2,14-dithiolate) and $\mathbf{L'}^{2-}$ (2,12-dimethyl-3,7,11-triaza-2,11-tridecadiene-1,13-dithiolate) are denoted as $[S_2{}^{Me2}N_3(Pr,Pr)]^{2-}$ and $[S_2N_2(Pr,Pr)]^{2-}$ elsewhere.[16] In $\mathbf{FeL(N_3)}$, azide is trans to a thiolate.[16] (b) Iron coordination in the crystal structure of the α subunit of *Rhodococcus* sp. R312 NH_{lt}.[3] Amino acid side chains from noncoordinating residues are omitted.

In the dark, *Rhodococcus* sp. N-771 and sp. R312 produce an inactive form of nitrile hydratase (NH_{dk}) that is activated by

† Haverford College.

‡ University of Washington.

§ DuPont. Contribution No. 7671 from Central Research and Development.

(1) Yamada, H.; Kobayashi, M. *Biosci. Biotechnol. Biochem.* **1996**, *60*, 1391−1400.

(2) Abbreviations used: ENDOR, electron nuclear double resonance; EPR, electron paramagnetic resonance; EXAFS, extended X-ray absorption fine structure (XAS above edge); FF, Fourier filtered; FT, Fourier transform; IR, infrared; L and L′, see Figure 1; N′, nitrogen atom of nitrosyl ligand; NH_{dk}, nitrile hydratase prepared in the dark; NH_{lt}, nitrile hydratase prepared in the light; *N*-MeIm, *N*-methylimidazole; OEP, octaethylporphyrin; *o*-phen, 1,10-phenanthroline; TACN, 1,4,7-trimethyl-1,4,7-triazacyclononane; TMC, 1,4,8,11-tetramethyl-1,4,8,11-tetraazacyclotetradecane; XANES, X-ray absorption near edge spectrum (XAS in edge region); XAS, X-ray absorption spectroscopy or spectrum.

(3) Huang, W.; Jia, J.; Cummings, J.; Nelson, M.; Schneider, G.; Lindqvist, Y. *Structure* **1997**, *5*, 691−699.

(4) Scarrow, R. C.; Brennan, B. A.; Cummings, J. G.; Jin, H.; Duong, D. J.; Kindt, J. T.; Nelson, M. J. *Biochemistry* **1996**, *35*, 10078−10088.

(5) Sugiura, Y.; Kuwahara, J.; Nagasawa, T.; Yamada, H. *J. Am. Chem. Soc.* **1987**, *109*, 5848−5850.

(6) Jin, H.; Turner, I. M., Jr.; Nelson, M. J.; Gurbiel, R. J.; Doan, P. E.; Hoffman, B. M. *J. Am. Chem. Soc.* **1993**, *115*, 5290−5291.

(7) Doan, P. E.; Nelson, M. J.; Jin, H.; Hoffman, B. M. *J. Am. Chem. Soc.* **1996**, *118*, 7014−7015.

S0002-7863(97)03291-5 CCC: $15.00
Published on Web 08/29/1998

exposure to near-UV light.[8−10] Difference FT-IR and resonance Raman spectroscopies suggest that NH_{dk} has nitric oxide coordinated to the iron,[11,12] and EPR spin-trapping experiments indicate release of one NO per iron center during photoactivation.[10] The coordinated NO is evident in the 1.7 Å crystal structure of the dark form of the nitrile hydratase from *Rhodococcus* sp. N-771.[13] The nitrile hydratase from *Comamonas testosteroni* NI1, which has a different amino acid sequence, has recently been shown to undergo the same type of photoactivation with release of nitric oxide. For both this enzyme and that from *Rhodococcus* sp. R312, the photoactivation was shown to be reversed by addition of stoichiometric (1:1 with respect to iron) nitric oxide.[14] Our previous XAS study[4] of light-activated nitrile hydratase (NH_{lt}) from *Rhodococcus* sp. R312 found no evidence for the short Fe−N bonds (1.6−1.8 Å) characteristic of nitric oxide ligation,[15] showing that at most a very small fraction (<20%) of NO remains bound to the iron after activation.

We have obtained and analyzed the iron K-edge X-ray absorption spectrum (XAS) of the "dark", inactive form of nitrile hydratase (NH_{dk}) from *Rhodococcus* sp. R312. The presence of the iron−nitrosyl bond in NH_{dk} has a major effect on the EXAFS, and from the analysis we are able to determine both the Fe−N′ bond length (we use N′ to denote the nitrosyl nitrogen) and ∠FeN′O. For comparison, and to validate our EXAFS analysis techniques, we report XAS analyses of a mixed thiolate/nitrogen-ligated iron(III) complex $\mathbf{FeL}^+$ (Figure 1a), its low-spin six-coordinate azide and nitrosyl adducts ($\mathbf{FeL(N_3)}$ and $\mathbf{FeL(NO)}^+$), and the high-spin iron (II) species ($\mathbf{Fe^{II}L'}$).[16] The XAS of $\mathbf{FeL(N_3)}$ and $\mathbf{FeL(NO)}^+$ closely mimic the spectra of butyrate-stabilized active nitrile hydratase (NH_{lt}) and NH_{dk}, respectively.

Experimental Section

Syntheses of $\mathbf{[FeL](PF_6)}$ and $\mathbf{FeL(N_3)}$ are described elsewhere, along with their single-crystal X-ray structures.[16] The synthesis and structure of $\mathbf{Fe^{II}L'}$ will be described in detail in a separate paper (Shoner, S. C.; Nienstedt, A. M.; Kung, I.; Barnhart, D.; Kovacs, J. A. Submitted to *Inorg. Chem.*).

Nitrosyl(2,3,13,14-tetramethyl-4,8,12-triaza-3,12-pentadecadiene-2,14-dithiolato)iron(1+) Hexafluorophosphorate, $\mathbf{[FeL(NO)](PF_6)}$. On a high-vacuum line, 1.15 equiv (in a calibrated 50-mL bulb) of NO gas was added to a frozen MeCN solution of $\mathbf{[FeL](PF_6)}$. The resulting solution was allowed to warm to ambient temperature and then overlayed with 90 mL of Et_2O to afford crystalline $\mathbf{[FeL(NO)](PF_6)}$ after 2 days at −35 °C. All volatiles were then removed under vacuum to afford $\mathbf{[FeL(NO)](PF_6)}$ as a dark black solid. Anal. Calcd for $FeC_{16}H_{31}ON_4S_2PF_6$: C, 34.29; H, 5.58; N, 10.00; S, 11.45; O, 2.86. Found: C, 33.83; H, 5.88; N, 9.63; S, 12.01; O, 5.93. IR: ν (cm^{-1}) 1822 (NO), 1615 (C=N). The Mössbauer and magnetic properties of $\mathbf{[FeL(NO)](PF_6)}$ will be described in more detail in a separate paper (Popescue, V.-C.; Münck, E.; Krebs, C.; Pereira, A.; Tavares, P.; Huynh, B. H.; Schweitzer, D.; Ellison, J. J.; Kovacs, J. A.; Cummings, J. G.; Turner, I. M., Jr.; Nelson, M. J. Manuscript in preparation).

NH_{dk} from *Rhodococcus* sp. R312. Cell growth, protein purification, and sample loading were carried out in the dark, but otherwise followed the same procedures used to prepare the earlier NH_{lt} sample.[17] Prior to loading in the sample holder, the protein was dialyzed and concentrated in pH 7.0 buffer with 0.1 M *N*-(2-hydroxyethyl)piperazine-*N*-2-ethanesulfonic acid (pH 7.0 at 4 °C) and 0.04 M sodium butyrate.[18] Activity measurements indicated that the sample was less than 5% light activated at the time of loading.

XAS Data Collection. Spectra of model complexes $Fe(Et_2NCS_2)_3$, $[Fe(o\text{-phen})_3][ClO_4]_2$, and $[Fe(N\text{-MeIm})_3][BF_4]_2$ are the same as used in previous studies[19,20] and were obtained in transmission mode using powders diluted with boron nitride. All other spectra (including that of NH_{lt} which has been previously reported[4,18]) were obtained at the National Synchrotron Light Source, beam line X9b, using energy-discriminated fluorescence detection. A manganese filter was placed between the sample and fluorescence detector to selectively attenuate the scattering signal.[4] Energy calibration employed the first inflection point of iron foil (7111.2 eV[21]) or (equivalently) the 7113.0 eV pre-edge peak of $[Et_4N][FeCl_4]$.[22] Spectra of ground crystalline $\mathbf{[FeL](PF_6)}$, $\mathbf{FeL(N_3)}$, $\mathbf{[FeL(NO)](PF_6)}$, and $\mathbf{Fe^{II}L'}$ (diluted with BN) were obtained at room temperature using fluorescence detection. The NH samples were cooled in the dark under vacuum to ca. 20 K, using a helium Displex cryostat.

The fluorescence data were converted to edge-normalized XANES and EXAFS data by applying corrections for energy-dependent detector efficiency, air and window absorption, self-absorption, and K-shell absorption cross-section.[19] The simulation of the edge and baseline followed the procedures used earlier with NH_{lt} samples.[4] The EXAFS (χ) is multiplied by k^n and plotted as a function of k, where

$$k = [2m_e(E - 7125\ \text{eV})]^{1/2}/\hbar \quad (1)$$

EXAFS Spectral Simulations. Simulations used the single-scattering EXAFS eq 2, where each shell consists of n_i atoms of the same type with an Fe-X distance of r_i and a variability (disorder) in these Fe−X distances given by σ^2.

$$\chi_{calc} = \sum_{i=1}^{\text{no. of shells}} n_i f_i k_i^{-1} r_i^{-2} \exp(-2\sigma^2 k_i^2) \sin(2k_i r_i + \alpha_i) \quad (2)$$

where

$$k_i = [2m_e(E - (7125\ \text{eV} + \Delta E_i))]^{1/2}/\hbar \quad (3)$$

The amplitude function, f_i, includes mean-free path effects, and the phase function, α_i, is the sum of scattering atom and central atom phase shifts; both are functions of k_i.[23] E is the energy of the incident photon, and ΔE_i is an adjustable parameter indicating the difference between the true ionization energy of the K-shell electron and 7125 eV, the nominal edge energy used in eq 1.

FEFF version 7.02[23−25] was used with the crystal structure of $\mathbf{FeL(N_3)}$[16] to calculate f_i and α_i (eq 2) for Fe−N and Fe−S scattering. From

(8) Nagamune, T.; Kurata, H.; Hirata, M.; Honda, J.; Koike, H.; Ikeuchi, M.; Inoue, Y.; Hirta, A.; Endo, I. *Biochem. Biophys. Res. Commun.* **1990**, *168*, 437−442.

(9) Nagamune, T.; Kurata, H.; Hirata, M.; Honda, J.; Hirta, A.; Endo, I. *Photochem. Photobiol.* **1990**, *51*, 87−90.

(10) Odaka, M.; Fujii, K.; Hoshino, M.; Noguchi, T.; Tsujimura, M.; Nagashima, S.; Yohda, M.; Nagamune, T.; Inoue, Y.; Endo, I. *J. Am. Chem. Soc.* **1997**, *119*, 3785−3791.

(11) Noguchi, T.; Honda, J.; Nagamune, T.; Sasabe, H.; Inoue, Y.; Endo, I. *FEBS Lett.* **1995**, *358*, 9−12.

(12) Noguchi, T.; Hoshino, M.; Tsujimura, M.; Odaka, M.; Inoue, Y.; Endo, I. *Biochemistry* **1996**, *35*, 16777−16781.

(13) Nagashima, S.; Nakasako, M.; Dohmae, N.; Tsujimura, M.; Takio, K.; Odaka, M.; Yohda, M.; Kamiya, N.; Endo, I. *Nat. Struct. Biol.* **1998**, *5*, 347−351.

(14) Bonnet, D.; Artaud, I.; Moali, C.; Petre, D.; Mansuy, D. *FEBS Lett.* **1997**, *409*, 216−220.

(15) Enemark, J. H.; Feltham, R. H. *Coord. Chem. Rev.* **1974**, *13*, 339−406.

(16) Ellison, J. J.; Nienstedt, A. M.; Shoner, S. C.; Barnhart, D.; Cowen, J. A.; Kovacs, J. A. *J. Am. Chem. Soc.* **1998**, *120*, 5691−5700.

(17) Brennan, B. A.; Cummings, J. G.; Chase, D. B.; Turner, I. M., Jr.; Nelson, M. J. *Biochemistry* **1996**, *35*, 10067−10077.

(18) The buffer used for NH_{dk} is pH 7.0 at 4 °C and is the same as used for the NH_{lt} sample that was previously reported[4] as pH 7.3; the latter value is correct for the pH of the buffer at 25 °C.

(19) Scarrow, R. C.; Trimitsis, M. G.; Buck, C. P.; Grove, G. N.; Cowling, R. A.; Nelson, M. J. *Biochemistry* **1994**, *33*, 15023−15035.

(20) Seefeldt, L. C.; Ryle, M. J.; Lanzilotta, W. N.; Scarrow, R. C.; Jensen, G. M. *J. Biol. Chem.* **1996**, *271*, 1551−1557.

(21) Bearden, J. A.; Burr, A. F. *Rev. Mod. Phys.* **1967**, *39*, 78−124.

(22) Scarrow, R. C.; Maroney, M. J.; Palmer, S. M.; Que, L., Jr.; Roe, A. L.; Salowe, S. P.; Stubbe, J. *J. Am. Chem. Soc.* **1987**, *109*, 7857−7864.

(23) Rehr, J. J.; de Leon, J. M.; Zabinsky, S. I.; Albers, R. C. *J. Am. Chem. Soc.* **1991**, *113*, 5135−5140.

(24) Ankoudinov, A. L. Ph.D. Thesis, University of Washington, 1996.

the atomic coordinates, FEFF calculates $\chi_{path}(k)$ for each scattering pathway. Each χ_{path} is output in a "chip000x.dat" file that also contains "magnitude" and "phase" columns, from which we calculate, for use in eq 2, f_i = ("magnitude")kr_X^2 and α_i = "phase" $- 2kr_X$. The f_i and α_i depend slightly on the bond length (r_i), and we modeled this variation as $f_i = f_0 + r_i f_1$, and $\alpha_i = \alpha_0 + r_i\alpha_1$. The f_0, f_1, α_0, and α_1 functions for Fe−N and Fe−S bonds were generated using "chip000x.dat" files for the shortest and longest bonds of each type found in **FeL(N$_3$)**.[16] These functions of k are given in Table S1.[26] The f_i and α_i functions for nonbonded (ca. 3 Å) Fe−C and Fe−O interactions were generated in a similar manner. Since no such Fe−O paths are present in **FeL(N$_3$)**, and because we are interested in modeling possible S-bound sufinate and sulfenate coordination to the iron (vide infra), we used coordinates of bis(2-((2-pyridylmethyl)amino)ethylsulfinato)cobalt(III) perchlorate dihydrate[27] as the basis for these calculations. The cobalt(III) was replaced by an iron(III) ion; the virtual identity of the ionic radii[28] for these low-spin ions ensures that this is a reasonable substitution. The FEFF calculations for this hypothetical iron complex with sulfinate ligation was used to confirm that multiple scattering paths (such as Fe−S−O−Fe) would not contribute significantly to the EXAFS because of the low (≈115°) ∠FeSO.

FEFF 7.02 was also used to generate f and α functions that describe single and multiple scattering EXAFS arising from the FeN′O unit. A set of 36 "reference spectra" (including the spectra from individual paths) were calculated by replacing the azide in the crystallographic coordinates of **FeL(N$_3$)** by an NO group with various $r_{N'}$ (1.65, 1.60, or 1.70 Å), $r_{N'O}$ (1.15, 1.12, or 1.18 Å), and ∠FeN′O (160°, 150°, 170°, or 180°). The atomic potentials and phase shifts for each atom type were calculated using the first values listed; because of its unusually short bond to iron, a separate potential was calculated for the nitrosyl nitrogen; for clarity, we will often refer to this nitrogen as N′. As expected, the single scattering χ_{path} for the short Fe−N′ bond was found to depend only on $r_{N'}$, but differed slightly from that predicted by the Fe−N scattering functions of Table S1. The method of the previous paragraph was used to determine f_0, f_1, α_0, and α_1 functions for the Fe−N′ bond (see Table S2).

For each of the 36 geometries, the calculated EXAFS due to Fe−O−Fe, Fe−N′−O−Fe, and Fe−N′−O−N′−Fe scattering were summed and used to generate parametrized $f_{Fe(N')O}$ and $\alpha_{Fe(N')O}$ functions that can be used with eq 2 to simulate the EXAFS from these three paths. To retain the magnitude and phase information of "chip000x.dat" files, the complex values {"magnitude" × exp(i "phase")} were summed to obtain a χ_{cmplx} for the three paths. (The χ_{cmplx} is calculated by FEFF; the "mag" and "phase" columns of the FEFF output files are χ_{cmplx} represented in polar coordinates and the predicted observable χ = Im(χ_{cmplx}).[29]) We then sought $f_{Fe(N')O}$ and $\alpha_{Fe(N')O}$ functions that would best approximate the χ_{cmplx} according to eq 4.

$$\chi_{cmplx} \approx f_{Fe(N')O} k^{-1} r_{N'}{}^{-2} \exp(i[2kr_{N'} + \alpha_{Fe(N')O}]) \qquad (4)$$

Changes in χ_{cmplx} were approximately linear with changes in $r_{N'}$ and $r_{N'O}$, but nonlinear with respect to changes in ∠FeN′O, with only slight changes caused by a change from 180° and 170° but progessively larger changes with changes to 160° or 150°. The following functional form was found to be effective, when used with eq 4, in reproducing both the 36 "reference" spectra and subsequent EXAFS simulations performed for other geometries:

$$F_{Fe(N')O} = F_0 + r_{N'}F_1 + r_{N'O}F_2 + \theta^2 F_3 + \theta^4 F_4, \qquad F = f \text{ or } \alpha;\ \theta = 180° - \angle FeN'O \quad (5)$$

The least-squares fitting of χ_{cmplx} to eq 4 was performed successively with k values every 0.05 Å^{-1} from 0 to 20 Å^{-1}. At each k, the 10 values of the f_n and α_n functions were refined starting with the values from the previous value of k (this prevented "phase wrapping" of the α functions). The values of the f_n and α_n functions are given in Table S3.

In computing the EXAFS from the XAS, we used 7125 eV (an energy close to the top of the iron K-edge) for the ionization energy of the Fe 1s atom (see eq 1). To align the FEFF simulations with our data, we adjusted the value of ΔE_i used in eq 3. A good simulation of the room-temperature EXAFS spectrum of **FeL(N$_3$)** was obtained using T = 300 K and Debye temperature = 700 K to approximate vibrational disorder,[25] and no amplitude reduction factor was required. A least-squares alignment between the theoretical and observed EXAFS spectra determined ΔE_i. Values within the range −0.1 to −0.7 eV were obtained for fits to $k\chi$, $k^2\chi$, $k^3\chi$, and Fourier-filtered $k^3\chi$ (Figure S1 and caption). As a result of these fits, $\Delta E_i = -0.5$ eV was used in the subsequent analyses; the same value was used for all shells. The least-squares residual was most uniform from low k to high k for fits to $k^2\chi$ or the Fourier-filtered $k^3\chi$, and thus fits to these types of data are emphasized.

Least-Squares Fits to EXAFS Spectra. The Fourier-filtered $k^3\chi$ were fit using established procedures.[4,19] Fourier filtering of $k^3\chi$ (k = 1.0−14.3 Å^{-1} with 5% windowing; r' = 1.0−2.3 Å for Tables 1 and S1 and Figure 3) isolates EXAFS contributions from first-sphere atoms, and an empirical weighting scheme is used to estimate the reproducibility of the Fourier-filtered data ((k × Å, σ_{data} × Å^3) pairs: (2.2, 0.14), (4, 0.19), (8, 0.26), (10, 0.42), (13, 0.88), (14.3, 0.56)). For the fits to Fourier-filtered $k^3\chi$ of NH_{dk} and **FeL(NO)**$^+$ shown in Tables S5 and S6, the back-transform range is expanded to r' = 1.0−2.7 Å to include features from the second coordination sphere.

Except as noted in Table S4, reported least-squares residuals and uncertainty estimates follow recommendations of the International Workshops on Standards and Criteria in XAFS.[30] The minimized residual is R^2, the average of $[(y_{data} - y_{calc})/\sigma_{data}]^2$ between k = 2.2 and 14.3 Å^{-1}. It is reported as $\epsilon^2 = [n_{idp}/(n_{idp} - n_p)]R^2$, where y is $k^2\chi$ or Fourier transformed $k^3\chi$, n_p is the number of refined parameters, and n_{idp} is the number of data points for $k^2\chi$ fits. For Fourier filtered fits, $n_{idp} = 10.1 = 2\,\Delta k\,\Delta r'/\pi$ (except for Table S5 and S6 fits, where n_{idp} = 13.5). Refined values are reported with uncertainties (of last digit; in parentheses[31]), indicating the range over which ϵ_ν^2 increases by 1.[30] For fits to $k^2\chi$, we used σ_{data} = 0.05, an approximation based on noise levels at high k and baseline error at low k; see, for example, Figure S1.[26]

Results

EXAFS Simulations. Rehr and co-workers suggest using coordinates of chemically similar coordination environments with their FEFF software to determine amplitude and phase functions for EXAFS analysis.[23] Several of our previous EXAFS studies,[19,20] including one of iron coordination in nitrile hydratase,[4] used calculations by versions 5 and 6 of FEFF with coordinates of high-spin compounds, $Fe(im)_6^{2+}$ and $[Fe_4S_4(SCH_2CH_3)_4]^{2-}$. We have now used the most recent version (7.02) of FEFF[24,25] to generate new amplitude and phase functions for Fe−N and Fe−S scattering (Table S1), based upon the crystal structure of the low-spin iron(III) model compound **FeL(N$_3$)**.

Table 1 compares fits to EXAFS of a variety of simple iron(II) and iron(III) complexes (both high- and low-spin). The new functions give better fits (lower ϵ^2) to the EXAFS of the sulfur-containing model complexes. The new functions have

(25) Zabinsky, S. I.; Rehr, J. J.; Ankudinov, A.; Albers, R. C.; Eller, M. J. *Phys. Rev. B* **1995**, *52*, 2995−3009.

(26) Tables S1−S6 and Figure S1 are Supporting Information. See statement at end of paper.

(27) Lundeen, M.; Firor, R. L.; Seff, K. *Inorg. Chem.* **1978**, *17*, 701−706.

(28) Shannon, R. D. *Acta Crystallogr., Sect. A* **1976**, *32*, 751−767.

(29) Mustre de Leon, J.; Rehr, J. J.; Zabinsky, S. I.; Albers, R. C. *Phys. Rev. B* **1991**, *44*, 4146−4156.

(30) Bunker, G., Hasnain, S., Sayers, D., Eds. In *X-ray Absorption Fine Structure*; Hasnain, S. S., Ed.; Ellis Horwood: New York, 1991; pp 751−770.

(31) Uncertainty estimates are reported in parentheses following the value and are expressed as uncertainty of the last reported digit. In cases where the uncertainty range is asymmetric about the most likely value, separate + and − values are given for the uncertainty.

Table 1. Refined Parameters Obtained from Fits to EXAFS of Model Complexes Using Amplitude and Phase Functions Used Previously or the New Functions Generated for This Study[31] [a]

	fit to (f and α)		
	FF $k^3\chi$ (previous)[b]	FF $k^3\chi$ (new)[c]	$k^2\chi$ (new)[c]
	$Fe(Et_2NCS_2)_3$ (80 K)		
n (6)	6.4(5)	5.6(5)	5.4(7)
r/Å (2.307)[32]	2.316(3)	2.311(3)	2.309(5)
σ^2/Å^2	0.0016(8)[d]	0.0045(8)	0.0041(10)
ϵ^2	9.5	5.7	16
	$Fe(Et_2NCS_2)_3$		
n (6)	6.8(9)	5.9(8)	6.0(14)
r/Å (2.357)[32]	2.356(6)	2.347(6)	2.345(11)
σ^2/Å^2	0.008(2)[d]	0.012(2)	0.012(3)
ϵ^2	8.9	6.7	21
	$Fe(o\text{-phen})_3(ClO_4)_2$		
n (6)	5.2(6)	5.0(6)	6.0(9)
r/Å (1.978)[33]	1.980(6)	1.977(5)	1.978(9)
σ^2/Å^2	−0.002(1)[d]	0.003(1)	0.005(2)
ϵ^2	9.4	9.1	15
	$[Fe(N\text{-MeIm})_6][BF_4]_2$		
n (6)	5.4(10)	5.2(10)	5.4(14)
r/Å (2.20 ± 0.01)[e]	2.204(10)[d]	2.185(10)	2.188(17)
σ^2/Å^2	0.002(3)[d]	0.007(3)	0.008(4)
ϵ^2	3.8	2.1	13
	FeL^+		
n_N (3; $n_S = 5 - n_N$)[f]	3.0(5)	3.1(5)	3.4(8)
r_N/Å (1.990)[16]	2.018(25)	2.021(25)	2.009(40)
r_S/Å (2.147)[16]	2.156(15)	2.155(16)	2.157(22)
σ^2_N/Å^2	0.003(6)[d]	0.009(8)	0.009(8)
σ^2_S/Å^2	0.002(4)[d]	0.005(4)	0.005(5)
ϵ^2	5.3	3.7	5.9
	$FeL(N_3)$		
n_N (4; $n_S = 6 - n_N$)[f]	3.7(5)	3.8(5)	4.0(8)
r_N/Å (2.042)[16]	2.06(2)	2.06(2)	2.05(4)
r_S/Å (2.203)[16]	2.19(2)	2.19(2)	2.19(2)
σ^2_N/Å^2	0.004(7)[d]	0.011(9)	0.012(9)
σ^2_S/Å^2	0.002(3)[d]	0.005(3)	0.005(4)
ϵ^2	4.4	2.9	6.2
	$Fe^{II}L'$		
n_N (3; $n_S = 5 - n_N$)[f]	3.2(6)	3.1(5)	3.3(9)
r_N/Å (2.177)[16]	2.184(28)	2.18(3)	2.17(5)
r_S/Å (2.353)[16]	2.347(14)	2.340(11)	2.344(20)
σ^2_N/Å^2	0.003(4)[d]	0.012(6)	0.009(7)
σ^2_S/Å^2	0.001(3)[d]	0.004(2)	0.004(4)
ϵ^2	4.1	3.4	8.7
	NH_{lt} (pH 7.0)[18]		
n_N ($n_S = 6 - n_N$)[f]	3.3(6)	3.4(6)	3.6(9)
r_N/Å (1.99)[4]	2.002(15)	2.008(18)	2.005(29)
r_S/Å (2.21)[4]	2.213(10)	2.204(9)	2.206(16)
σ^2_N/Å^2	0.000(2)[d]	0.006(3)	0.007(3)
σ^2_S/Å^2	0.002(2)[d]	0.006(2)	0.005(3)
ϵ^2	1.4	0.55	4.1

[a] Also shown is a comparison between fits to Fourier-filtered $k^3\chi$ and those to $k^2\chi$. Bond lengths in parentheses are from published crystal structure or, for NH_{lt}, a previous EXAFS study. [b] Fitting as in previous publications,[4,19,20,34,35] using f_i and α_i generated by FEFF 5 or FEFF 6, except that Fe−S amplitude functions (f_S) were multiplied by an empirical reduction factor of 0.75. $\Delta E_i = 0$ eV for Fe−N and $\Delta E_i = -3$ eV for Fe−S. These parameters were established by studies with model complexes. [c] Using new f_i and α_i (Table S1) generated by FEFF 7.02. No amplitude reduction factor was used, and $\Delta E_i = -0.5$ eV for both Fe−N and Fe−S scattering. [d] Previous (but not new) amplitude functions include vibrational disorder predicted by FEFF 5 or FEFF 6 (for $T = 100$ K and Debye $T = 700$ K; $\sigma^2_{vib} \approx 0.004$ Å^2); thus, the refined σ^2 is the extent to which the disorder exceeds that predicted by FEFF. [e] No crystal structure exists for BF_4 salt; other salts of $[Fe(N\text{-MeIm})_6]^{2+}$ have r_N(av) = 2.190 Å (−78 °C),[36] 2.197 Å,[37] and 2.207 Å.[38] [f] In fits to EXAFS of iron complexes of **L**, the total coordination number was constrained. Otherwise, n_N and n_S do not refine to correct values. For instance, for fits to $k^2\chi$ of **FeL(N$_3$)**, two minima exist; one has total coordination number 4 (3.1 Fe−N @ 2.00 Å with $\sigma^2 = 0.004$ Å^2 and 0.9 Fe−S @ 2.22 Å with $\sigma^2 = 0.000$ Å^2; $\epsilon^2 = 6.5$), while the other has total coordination number 10 (7 Fe−N @ 2.11 Å with $\sigma^2 = 0.02$ Å^2 and 3 Fe−S @ 2.19 Å with $\sigma^2 = 0.007$ Å^2; $\epsilon^2 = 5.4$).

the further advantage that no empirical amplitude reduction is required and the same ΔE_i gives crystallographic Fe−X distances for both X = N and S. The chemically relevant refined bond lengths (r) and number of scatterers (n) are virtually identical to those obtained with the previously used functions. Thus, no revision is required of our previously published EXAFS analyses of nitrile hydratase. Table S4 shows parameters from additional fits to $k\chi$ (which emphasize low-k data) and $k^3\chi$ (which emphasize high-k data); the refined parameters are almost identical, suggesting that the new functions well-describe the EXAFS throughout the k range investigated. The refined r and n in Tables 1 and S4 are generally within ±0.02 Å and ±1 of the crystallographic values; these are reasonable confidence intervals for EXAFS analysis.[39] The only exceptions are the r_N distances from fits to Fourier-filtered $k^3\chi$ of **FeL**$^+$, but we note that, for these particular distances, the uncertainties indicated by the least-squares analysis are relatively large (±0.025 Å) due in part to correlations with n_N and r_S.

We also used FEFF to generate amplitude and phase functions describing single and multiple scattering from a nitrosyl bound to iron (Tables S2 and S3). Separate functions were generated for the Fe−N′ single scattering and for $\chi_{Fe(N')O}$, by which we denote the single and multiple scattering paths involving the nitrosyl oxygen. The $f_{Fe(N')O}$ and $\alpha_{Fe(N')O}$ functions which account for $\chi_{Fe(N')O}$ were parametrized as functions of $r_{N'}$, $r_{N'O}$, and ∠FeN′O according to eq 5 and were determined from FEFF simulations for a variety of Fe−N−O geometries, using eq 4 as described in the Experimental Section. In practice it was found that $r_{N'O}$ could not be well determined from EXAFS data, and so it was fixed to a value of 1.15 Å based on crystal structures found in the Cambridge Structural Database.[40] Furthermore, the σ^2 for the outer-sphere nitrosyl scattering was assumed to be $\sigma_{N'}^2 + 0.001$ Å^2 in order to limit the number of refined parameters.

X-ray Absorption Spectra. The change in the XAS data (and, by inference, the iron coordination environment) upon light activation of nitrile hydratase is obvious and much greater than the small differences between the spectra of active NH_{lt} prepared at pH 7.0[18] and inactive NH_{lt} prepared at pH 9.0.[4] Figure 2 compares the previously published iron K-edge XAS of active NH_{lt} with that of NH_{dk}. The edge features of NH_{dk} are shifted by about +1 eV compared to the corresponding features in NH_{lt}. A similar effect is seen on comparing the edge spectra of the model complexes **FeL(NO)**$^+$ and **FeL(N$_3$)** (Figure 2b,c). For instance the 1s → 3d pre-edge peak position in NH_{lt} is at 7111.9 eV, while that in NH_{dk} is at 7113.0 eV. The shift in edge energy indicates that the iron is more positively charged in the NO complexes, consistent with the $Fe^{4+}(NO^-) \leftrightarrow Fe^{3+}(NO)$ resonance forms of the {FeNO}^{6} electron count,[15] but inconsistent with the {FeNO}^{7} description. In a previous study of iron

(32) Leipoldt, J. G.; Coppens, P. *Inorg. Chem.* **1973**, *12*, 2269−2274.
(33) Koh, L. L.; Xu, Y.; Hsieh, A. K.; Song, B.; Wu, F.; Ji, L. *Acta Crystallogr., Sect. C* **1994**, *50*, 884−886.
(34) Brennan, B. A.; Alms, G.; Nelson, M. J.; Durney, L. T.; Scarrow, R. C. *J. Am. Chem. Soc.* **1996**, *118*, 9194−9195.
(35) Nelson, M. J.; Brennan, B. A.; Chase, D. B.; Cowling, R. A.; Grove, G. N.; Scarrow, R. C. *Biochemistry* **1995**, *34*, 15219−15229.
(36) Rauchfuss, T. B.; Dev, S.; Wilson, S. R. *Inorg. Chem.* **1992**, *31*, 153−154.
(37) Seel, F.; Lehnert, R.; Bill, E.; Trautwein, A. *Z. Naturforsch., B: Anorg. Chem., Org. Chem.* **1980**, *35*, 631−638.
(38) Miller, L. L.; Jacobson, R. A.; Chen, Y. S.; Kurtz, D. M., Jr. *Acta Crystallogr., Sect. C* **1989**, *45*, 527−529.
(39) Scott, R. A. *Methods Enzymol.* **1985**, *117*, 414−459.
(40) Allen, F. H.; Davies, J. E.; Galloy, J. J.; Johnson, O.; Kennard, O.; Macrae, C. F.; Mitchell, E. M.; Mitchell, G. F.; Smith, J. M.; Watson, D. G. *J. Chem. Inf. Comput. Sci.* **1991**, *31*, 187−204.

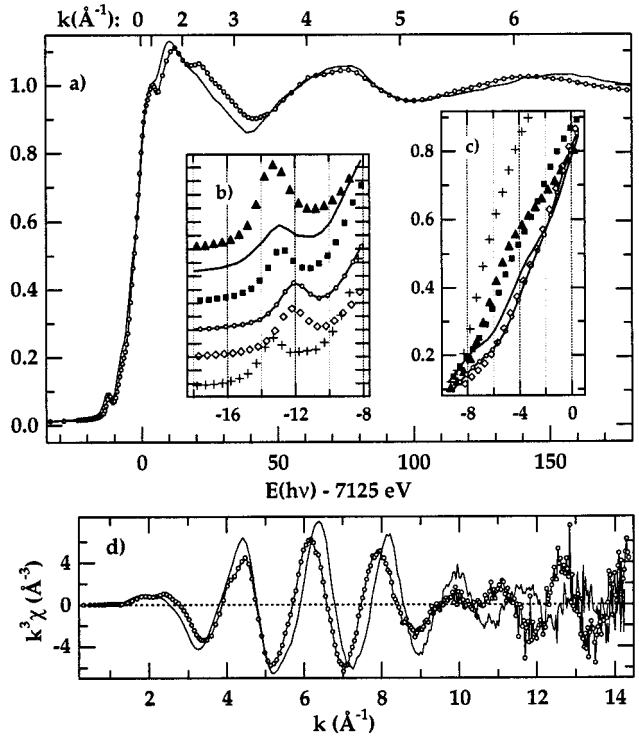

Figure 2. Comparison of Fe−K edge XAS for NH_{dk} (∘ ∘ ∘) and NH_{lt} (—). (a) Edge-normalized and baseline-corrected XANES obtained using a Si 220 monochromator. (b−c) Expansion of 1s → 3d peak and edge region, respectively, with XANES of model complexes: **FeL**$^+$ (▲), **FeL(N$_3$)** (■), **FeL(NO)**$^+$ (◇), and **Fe^{II}L′** (+). (d) $k^3\chi$. XANES of NH_{lt} at pH 7.8 (rather than the pH 7.0 data used elsewhere in this paper)[18] is used in a−c, so all compared spectra have similar energy resolution. Near-edge XAS are virtually unchanged between pH 7.0,[18] 7.8, and 9.0 samples.[4]

EDTA complexes,[41] the 1s → 3d pre-edge peak (cf. Figure 2b) is at 7112.7 eV for ferric EDTA, but shifts to 0.3 eV *lower* energy in the {FeNO}^{7} mixed iron complex of EDTA and NO, consistent with $Fe^{3+}(NO^-)$ (major) ↔ $Fe^{2+}(NO)$ (minor) resonance forms. The EPR silence of NH_{dk} is also consistent with the {FeNO}^{6} electron count.[10]

For iron complexes, the size of the 1s → 3d peak at ca. 7113 eV increases as the coordination number decreases.[42−44] Figure 2b shows that the 1s → 3d peaks in the nitrile hydratase spectra are similar in size to those of six-coordinate **FeL(N$_3$)** and **FeL-(NO)**$^+$ but are roughly one-half the size of the peak for five-coordinate **FeL**$^+$. This comparison supports six-coordinate iron in both NH_{lt} and NH_{dk} (at least in the frozen solutions used for the spectroscopic measurements). The pre-edge peak height of five-coordinate **Fe^{II}L′** is roughly comparable with that of the six-coordinate ferric models; this is consistent with the known smaller pre-edge peak areas of ferrous complexes[43] and is due in part to a greater degree of splitting of the 1s → 3d feature in ferrous compared to ferric complexes.[41,44]

The $k^3\chi$ EXAFS spectra of the NH_{lt} and NH_{dk} also differ substantially (Figure 2d). Figure 3 compares Fourier transforms

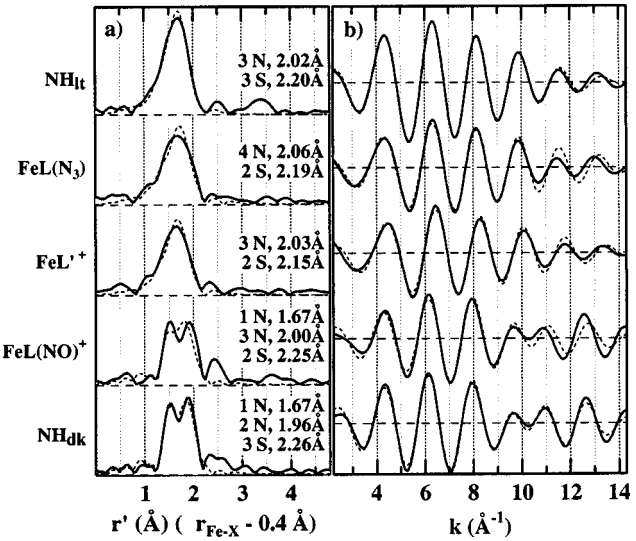

Figure 3. (a) Magnitude of Fourier transforms of $k^3\chi$ from $k = 1.0-14.3$ Å^{-1}. (b) First-sphere Fourier-filtered EXAFS obtained by back transformation between $r' = 1.0$ and 2.3 Å. Bond lengths and calculated spectra (- - -) are from simulations to the Fourier-filtered $k^3\chi$ using fixed integral n for each shell.[26]

(FT) and first-sphere Fourier-filtered EXAFS of NH_{lt} and NH_{dk} with those of model complexes **FeL**$^+$, **FeL(N$_3$),** and **FeL(NO)**$^+$. For this figure, Fourier filtering using back-transform limits of $r' = 1.0-2.3$ Å was used to isolate and compare first-sphere (directly bound atom) contributions to the EXAFS. The Fourier-filtered EXAFS of NH_{lt} is similar to that of **FeL(N$_3$),** while that of NH_{dk} resembles that of **FeL(NO)**$^+$. The latter two EXAFS spectra are unusual in showing minimal amplitude around $k = 10$ Å^{-1} and in having FT peaks at both $r' = 1.4$ and 1.9 Å, as well as smaller but significant intensity in the FT near 2.5 Å^{-1}.

EXAFS Analyses of NH$_{dk}$ and FeL(NO)$^+$. We used the new amplitude and phase functions to least-squares fit the EXAFS data for **FeL(NO)**$^+$ and NH_{dk}. An extensive list of fits is given in Tables S5 and S6.[26] The evolution of the EXAFS model and improvements in fits to the $k^2\chi$ of NH_{dk} are shown by Table 2, which lists refined parameters, and by Figure 4, which illustrates the fits. We began with a N_xS_{6-x} coordination model (fit **I**) as used for the fits to **FeL**$^+$, **FeL(N$_3$)**, **Fe^{II}L′**, and NH_{lt} data in Table 1. This simple model is unable to simulate the minimum in $k^2\chi$ or $k^3\chi$ amplitude around $k = 10$ Å^{-1} or the dual peaks at 1.5 and 1.9 Å in the $k^3\chi$ FT. Adding a third shell (a short Fe−N′ bond) allows us to reproduce these spectral features. Three shell fits to both data sets using $N'N_mS_{5-m}$ and $N'_2N_mS_{4-m}$ models with integral m were compared (fits 3−9 of Table S6); the best of these fits (fit **II**, Figure 4b; $\epsilon^2 = 6.7$) is that with the $N'N_3S_2$ ligand set, although the fit with $N'N_2S_3$ ligand set was only marginally worse ($\epsilon^2 = 6.9$). The refined short 1.68 Å Fe−N′ bond length is typical of nitrosyl coordination, and the refined Fe−N and Fe−S distances are about 0.05 Å shorter and 0.05 Å longer, respectively, than the refined distances for NH_{lt}. The bond lengths obtained by fitting to Fourier-filtered $k^3\chi$, using either $r' = 1.0-2.3$ Å (Figure 3) or $r' = 1.0-2.7$ Å (Table S6) were not significantly different from those obtained by fitting $k^2\chi$.

The fit to the $k^2\chi$ near $k = 10$ Å^{-1} in fit **II** is improved relative to fit **I** (Figure 4, part b vs part a), but the FT difference spectrum retains a relatively large peak at 2.3 Å^{-1}. Although it is possible to obtain some reduction in ϵ^2 by including a single-scattering second-sphere Fe−C shell (four atoms at 3.2 Å) or Fe−O shell (two atoms at 3.1 Å; fit **III**), these fits give only very small

(41) Zhang, Y.; Pavlosky, M. A.; Brown, C. A.; Westre, T. E.; Hedman, B.; Hodgson, K. O.; Solomon, E. I. *J. Am. Chem. Soc.* **1992**, *114*, 9189−9191.

(42) Roe, A. L.; Schneider, D. J.; Mayer, R. J.; Pyrz, J. W.; Widom, J.; Que, L., Jr. *J. Am. Chem. Soc.* **1984**, *106*, 1676−1681.

(43) Randall, C. R.; Shu, L.; Chiou, Y.-M.; Kagen, K. S.; Ito, M.; Kitajima, N.; Lachicotte, R. J.; Zang, Y.; Que, L., Jr. *Inorg. Chem.* **1995**, *34*, 1036−1039.

(44) Westre, T. E.; Kennepohl, P.; DeWitt, J. G.; Hedman, B.; Hodgson, K. O.; Solomon, E. I. *J. Am. Chem. Soc.* **1997**, *119*, 6297−6314.

Table 2. Results from Fits to Unfiltered $k^2\chi$ for NH_{dk}[a]

	fit no. (coord)						
	I (N_xS_{6-x})	**II**[b] ($N'N_3S_2$)	**III**[b] ($N'N_3S_2(O_n)$)	**IV**[c] ($N'N_3S_2$)	**V**[c] ($N'N_3S_2(O_n)$)	**VI**[c] ($N'N_2S_3$)	consensus[d]
$r_{N'}$/Å	*[x = 1.4(5)]*	1.680(30)	1.685(31)	1.684(27)	1.684(27)	1.680(27)	1.68(3)
r_N/Å	*2.18(4)*	1.975(22)	1.973(21)	1.977(20)	1.978(20)	1.968(25)	1.97(3)
r_S/Å	*2.228(13)*	2.265(12)	2.266(11)	2.267(11)	2.267(12)	2.265(11)	2.266(13)
$\sigma^2_{N'}$/Å^2		$0.002(^{+3}_{-2})$[a]	$0.003(^{+2}_{-3})$[a]	$0.003(^{+2}_{-3})$[a]	$0.002(^{+3}_{-2})$[a]	$0.003(^{+2}_{-3})$[a]	$0.003(^{+2}_{-3})$[a]
σ^2_N/Å^2	$0.000(^{+3}_{0})$[a]	$0.006(^{+5}_{-3})$	$0.005(^{+5}_{-2})$	$0.005(^{+5}_{-2})$	$0.005(^{+4}_{-2})$	$0.004(^{+5}_{-2})$	$0.005(^{+5}_{-3})$
σ^2_S/Å^2	*0.009(3)*	$0.003(^{+2}_{-1})$	$0.003(^{+2}_{-1})$	$0.003(^{+2}_{-1})$	$0.003(^{+2}_{-1})$	0.006(2)	
∠FeN′O/deg				$166(^{+14}_{-10})$	$164(^{+16}_{-11})$	$163(^{+17}_{-9})$	$164(^{+16}_{-11})$
n_O			4.2(30)[e]		$2.3(^{+38}_{-13})$[a,f]		
r_O			3.07(9)		3.15(16)		
ϵ^2	8.6	6.7	4.6	4.0	3.2	4.9	
ϵ^2(FF)[g]	11.1	10.7	7.3	3.8	0.4	4.4	

[a] Results from uncertainty mapping are shown in parentheses as uncertainties in last reported digit. For the fitting and uncertainty mapping, the following contraints were placed on the σ^2: that they be nonnegative, that the $\sigma_{N'}{}^2 \leq 0.005$ Å^2 (based on the assumption that disorder for the Fe-nitrosyl would be less than that for model complexes listed in Table 1), and, for fits **III** and **V**, that $0.005 \leq \sigma^2_{FeO} \leq 0.020$ Å^2 and $n_O \geq 1$. [b] Scattering involving the nitrosyl oxygen ($\chi_{Fe(N')O}$) was not modeled in fits **II** or **III**. [c] For fits **IV** to **VI**, the single and multiple scattering of the FeN′O unit is modeled using $r_{N'O} = 1.15$ Å and σ^2 (for paths involving the nitrosyl oxygen) fixed at $\sigma^2_{N'} + 0.001$ Å^2. [d] The uncertainty ranges of "consensus" values include the uncertainty ranges from fits **II** to **VI**. [e] When allowed to refine freely, σ^2_{FeO} refined to 0.03 Å^2; it was fixed at 0.02 Å for fit **III** in this table, in accordance with note *a*. [f] σ^2_{FeO} refined to 0.011 Å^2 for fit **V**. [g] ϵ^2 from corresponding fits to Fourier-filtered $k^3\chi$. Refined parameters are similar to those from fits to $k^2\chi$, and may be found in Table S6.

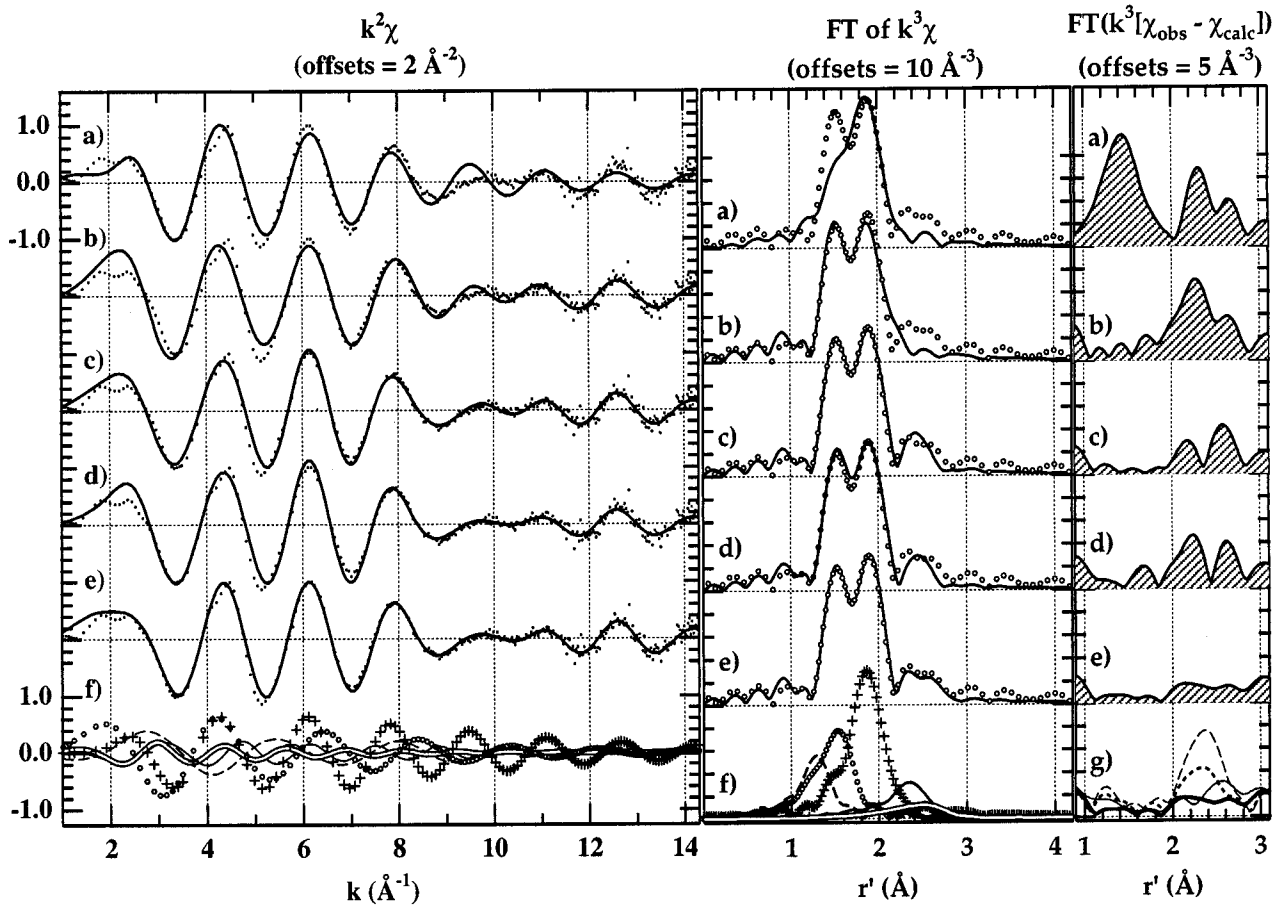

Figure 4. Fits to $k^2\chi$ of NH_{dk} using parameters of Table 2. For panels a−e, the left panel shows the data (• • •) and fits (—), the center panel shows the FT magnitude of $k^3\chi$ of the data (∘ ∘ ∘) and fits (—), and the right panel shows (at scale 2× the center panel) the FT magnitude of the residual spectra (data − fit): (a) fit **I** (N_xS_{6-x}, $\epsilon^2 = 8.6$); (b) fit **II** ($N'N_3S_2$, no modeling of $\chi_{Fe(N')O}$, $\epsilon^2 = 6.7$); (c) fit **IV** ($N'N_3S_2$, $\epsilon^2 = 4.0$); (d) fit **VI** ($N'N_2S_3$, $\epsilon^2 = 4.9$); (e) fit **V** ($N'N_3S_2(O_n)$, $\epsilon^2 = 3.2$); (f) left and center panels show individual shell contributions to fit **V**: N′ (- - -), N (∘ ∘ ∘), S (+ + +), $\chi_{Fe(N')O}$ (—), and the 3.1 Å O_n shell (═); (g) (right panel only) FT magnitude of residual spectrum as ∠FeN′O is varied in uncertainty mapping for fit **V**: 145° (— — —), 155° (- - -), 164° (bold solid line, refined value), and 175° (—).

features in the FT in the 2.1−2.5 Å region. The fit is improved more when the single and multiple scattering involving the nitrosyl oxygen[45] is included in the EXAFS model and the ∠FeN′O is refined, as it is in fit **IV** (Figure 4c). We denote these contributions to the EXAFS as $\chi_{Fe(N')O}$.

When the effects of $\chi_{Fe(N')O}$ are included in the modeling, the fits to the EXAFS of NH_{dk} are consistent with either $N'N_3S_2$ (fit **IV**; $\epsilon^2 = 4.0$) or $N'N_2S_3$ (fit **VI**; $\epsilon^2 = 4.9$) coordination to iron; the former model gives better fits, but the difference in ϵ^2 values is <1. The fits with either combination of ligands are

very similar (Figure 4c,d) and give virtually identical refined parameters, except for σ^2_S (Table 2). Refining the n in a fit to $k^2\chi$ (fit 10 of Table S6) gives $n_{N'} = 1.0$, $n_N = 3.0$, and $n_S = 2.0$; the uncertainty limits are $n_{N'} = 0.6-1.4$, $n_N = 1.9-3.8$, and $n_S = 1.2-3.3$. Even after inclusion of the $\chi_{Fe(N')O}$, the largest peaks in the difference FT occur around 2.5 Å. This suggests the presence of an additional shell of scatterers about 3 Å from the iron. We assumed that this was a single scattering shell of either carbon or oxygen atoms and started by assuming $\sigma^2 = 0.010$ Å (slightly larger than the first-sphere disorder factors; see Table S6) and then relaxed this condition to allow values between $\sigma^2 = 0.005$ and 0.020 Å. Adding a shell of about four carbon atoms at $r = 3.2$ Å dropped the ϵ^2 from 4.0 to 3.3 and reproduces the double hump in the $r' = 2.2-2.8$ Å region of the FT; an even slightly better fit ($\epsilon^2 = 3.2$) is obtained with a shell of about two oxygen atoms at 3.1 Å (fit **V** of Table 2 and Figure 4e). Because the drop in ϵ^2 (for $k^2\chi$ fits) upon addition of the Fe−C or Fe−O shell is less than 1, the uncertainty range for the refined n and r values for this shell is very large and includes $n = 0$, that is, the EXAFS data can only be said to be *suggestive* of the presence of a shell of scatterers at ca. 3.1 Å. Nevertheless, we include fit **V** in Table 2 because it shows that inclusion of the second-sphere single scattering shell does not significantly change the refined parameters (in particular the ∠FeN′O) for the other shells of the model.

Figure 4f shows that the FT of EXAFS from the various shells overlap substantially. This precludes the isolation of any one shell's EXAFS by Fourier filtering. Inclusion of the $\chi_{Fe(N')O}$ is needed for successful modeling of the features in the 2.0−2.7 Å region of the $k^3\chi$ FT of both NH_{dk} and **FeL(NO)**$^+$. Figure 5a shows that the dominant contribution to $\chi_{Fe(N')O}$ (for ∠FeN′O = 164°) is the double scattering path Fe−N′−O−Fe, while the triple and single scattering pathways give rise to smaller EXAFS with different phases and frequencies. Because of the differences in phase, the summed EXAFS from the three types of paths is smaller than that from the double scattering path alone.

A very similar sequence of fits was obtained for the **FeL(NO)**$^+$ spectrum. In this case the fits obtained with a $N'N_4S$ coordination model were generally somewhat better (lower ϵ^2) than the fits obtained assuming the correct coordination model of $N'N_3S_2$, as shown in Table 3. However, when a single scattering Fe−C shell is included in the model, the difference between the ϵ^2 values for the $N'N_4S(C_n)$ and $N'N_3S_2(C_n)$ models is insignificant (≈0.5; see Table S5). As in the case of NH_{dk}, inclusion of the outer-sphere single scattering shell decreases the ϵ^2 slightly but does not affect the other refined parameters significantly.

Figure 5b illustrates how the $\chi_{Fe(N')O}$ changes as a function of the ∠FeN′O. The four spectra are simulated using parameters from fit **V** of Table 2 (∠FeN′O = 164°) and during the course of uncertainty mapping for this fit (∠FeN′O = 175°, 155°, and 145°). The amplitude of the simulated $k^2\chi_{Fe(N')O}$ increases as the FeN′O unit becomes more linear, as generally observed for multiple scattering effects.[46] Figure 4g graphs the FT difference spectra from these fits and shows that effective simulation of the $r' = 2.0-2.6$ Å region of the FT requires ∠FeN′O ≈ 165°.

Figure 5b also illustrates the success of our amplitude and phase parametrization for $\chi_{Fe(N')O}$. The simulations using the parametrized functions are superimposable with the simulations using FEFF 7.02, except for the simulation with ∠FeN′O = 145°, which is outside the 150°−180° range of ∠FeN′O used for the parametrization. Even in that case the difference is slight.

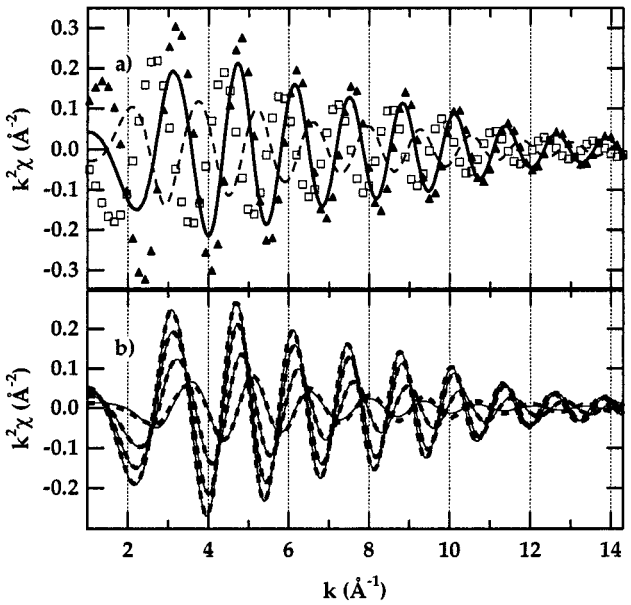

Figure 5. (a) Path contributions to $k^2\chi_{Fe(N')O}$ for ∠FeN′O = 164°. The Fe−O single scattering (− − −), Fe−O−N′−Fe double scattering (▲), and Fe−N′−O′-N′−Fe triple scattering (□) sum to give the $k^2\chi_{Fe(N')O}$ (—). (b) Variation in $k^2\chi_{Fe(N')O}$ during uncertainty mapping for fit **V** with ∠FeN′O fixed at 145° (smallest amplitude), 155°, 164° (refined value), and 175°. The dashed lines are calculations using the parametrized $f_{Fe(N')O}$ and $\alpha_{Fe(N')O}$ (as used in least-squares fitting); these overlay thinner solid lines representing $k^2\chi_{Fe(N')O}$ recalculated using FEFF 7.02 with geometrical parameters from the EXAFS fitting. These are visibly distinct only for the ∠FeN′O = 145° calculation.

Table 3. Results from Fits to Unfiltered $k^2\chi$ of $FeL(NO)^{+a}$

	$N'N_4S$	$N'N_3S_2$	$N'N_3S_2(C_n)$
$r_{N'}$/Å	1.685(27)	1.680(23)	1.689(28)
r_N/Å	1.999(19)	$1.998(^{+40}_{-27})$	$1.985(^{+34}_{-25})$
r_S/Å	2.273(16)	$2.267(^{+17}_{-23})$	$2.270(^{+14}_{-19})$
$\sigma^2_{N'}$/Å^2	$0.003(^{+2}_{-3})^a$	$0.002(^{+3}_{-2})^a$	$0.002(^{+3}_{-2})^a$
σ^2_N/Å^2	$0.008(^{+5}_{-3})$	$0.009(^{+9}_{-5})$	$0.007(^{+7}_{-3})$
σ^2_S/Å^2	$0.001(^{+2}_{-1})^a$	$0.005(^{+3}_{-2})$	0.005(2)
∠FeN′O/deg	$168(^{+12}_{-10})$	$165(^{+15}_{-9})$	$162(^{+18}_{-9})$
n_C			$4.1(37)^b$
r_C			3.04(12)
ϵ^2	5.0	6.2	5.2
ϵ^2(FF)^c	1.8	3.4	2.4

[a] The single and multiple scattering of the FeN′O unit is modeled as for fits **IV** to **VI** of Table 2: see notes *a* and *c* of that table. [b] When allowed to refine freely, σ^2_{FeC} refined to 0.04 Å^2; it was fixed at 0.02 Å for the $N'N_3S_2(C_n)$ fit and constained between 0.005 and 0.02 Å^2 for purposes of uncertainty mapping. [c] ϵ^2 from corresponding fits to Fourier-filtered $k^3\chi$. Refined parameters are similar to those from fits to $k^2\chi$ and may be found in Table S5.

For both NH_{dk} or for **FeL(NO)**$^+$, the refined bond distances and the ∠FeN′O do not change significantly if weighted Fourier-filtered $k^3\chi$ is fit instead of $k^2\chi$ (Tables S5 and S6). These also do not depend much upon the exact values of n_S or n_N, or upon the presence or absence of a ca. 3.1 Å Fe−C or Fe−O shell. The consensus $r_{N'} = 1.68(3)$ Å and $r_S = 2.27(2)$ Å for both NH_{dk} and **FeL(NO)**$^+$. The refined r_N is 1.97(3) Å for NH_{dk} and is about 0.03 Å longer for **FeL(NO)**$^+$; the difference is within the uncertainty limits. The uncertainty ranges for

(45) Westre, T. E.; Di Cicco, A.; Filipponi, A.; Natoli, C. R.; Hedman, B.; Solomon, E. I.; Hodgson, K. O. *J. Am. Chem. Soc.* **1994**, *116*, 6757−6768.

(46) Westre, T. E.; Di Cicco, A.; Fillipponi, A.; Natoli, C. R.; Hedman, B.; Solomon, E. I.; Hodgson, K. O. *J. Am. Chem. Soc.* **1995**, *117*, 1566−1583.

∠FeN′O span 153−180°, with the most likely values near 164° for both NH_{dk} and **FeL(NO)**$^+$.

Discussion

Comparisons and Analysis of XAS from Nitrile Hydratase and Models. The series of iron complexes using the pentadentate (two sulfur, three nitrogen atom) ligand **L** (Figure 1a) has proved valuable for the analysis of iron K-edge absorption spectra of both the light and dark forms of nitrile hydratase. The complexes **FeL(N$_3$)** and **FeL(NO)**$^+$ give iron K-edge absorption spectra which closely mimic those of NH_{lt} and NH_{dk}, suggesting similar coordination environments about iron. The crystallographically characterized model complexes (**FeL**$^+$, **FeL(N$_3$),** and **Fe^{II}L′**) were also useful in calibrating ΔE_i and in verifying that approximately correct (within ±0.02 Å or ±1) values of r_X and n_X can be obtained with our EXAFS fitting protocol.

The EXAFS fitting in this paper was accomplished with the aid of FEFF version 7.02. Table 1 shows that the amplitude and phase functions produced using FEFF 7.02 give better fits (lower residuals) relative to functions we generated using FEFF 5, particularly for sulfur-containing compounds. Importantly, the refined parameters do not differ significantly depending on whether the old or new functions are used (Table 1).[4]

EXAFS simulations and the data for NH_{dk} and **FeL(NO)**$^+$ show that a nitrosyl bound to iron contributes very low frequency ($r' \approx 1.3$ Å) EXAFS due to the short Fe−N′ bond. Inclusion of a ca. 1.7 Å Fe−X bond is required to satisfactorily fit the FT EXAFS in the 1.0−1.5 Å region (compare parts a and b of Figure 4). Such a bond is extremely short for iron complexes; aside from FeNO complexes, other precedents for such short FeX distances are ferryl (Fe^{4+}═O) containing complexes.[47−49] Unlike ferryl, the FeNO group gives rise to EXAFS multiple scattering involving the Fe−NO unit. This causes a peak in the FT EXAFS of NH_{dk} and **FeL(NO)**$^+$ with $r' \approx 2.4$ Å (Figures 3 and 4f,g). The ability of FEFF to model the multiple scattering EXAFS as a function of ∠FeN′O allows this angle to be determined from the data. Our parametrization of $\chi_{Fe(N')O}$ as a function of ∠FeN′O and $r_{N'}$ effectively reproduces the results of complete FEFF calculations (see, for instance, Figure 5b) and facilitates the least-squares fitting of EXAFS data. The functions given in Table S3 can be used in fitting EXAFS of other iron nitrosyl complexes.

Westre et al.[45] successfully used the GNXAS multiple-scattering analysis package[46] to model the EXAFS of five- and six-coordinate {FeNO}^{7} complexes. This analysis showed that the FeN′O scattering pattern was most pronounced for ∠FeN′O greater than about 150°. For [Fe(TMC)NO](BF$_4$)$_2$ (∠FeN′O = 178°) and Fe(TACN)(N$_3$)$_2$NO (∠FeN′O = 156°), the refined angles from GNXAS analysis were within 1° of the crystallographic values, which is impressive although perhaps fortuitous agreement; from analysis of the EXAFS of Fe(EDTA)(NO), which does not have a known crystal structure, Westre et al. claim ∠FeN′O = 156° ± 5°.[45] In the future, it will be valuable to compare our method of analysis using FEFF with that of the GNXAS package, taking advantage of the EXAFS data and crystal structures of **[FeL(NO)](PF$_6$)** (see below) and the {FeNO}^{7} complexes previously investigated.[45] By performing additional studies of model complexes and by obtaining higher quality EXAFS data on both **[FeL(NO)](PF$_6$)** and NH_{dk}, it may be possible to decrease the size of the uncertainty range for the ∠FeN′O.

Iron Coordination in NH_{lt} and NH_{dk}. Comparisons to the preedge XANES peak sizes for the ferric model complexes **FeL**$^+$, **FeL(N$_3$),** and **FeL(NO)**$^+$ allow us to assign coordination numbers of 6 for the iron in both NH_{lt} and NH_{dk}. In both cases, EXAFS fitting showed that two or three of the six ligand atoms are sulfur, with remaining coordination by nitrogen or oxygen atoms. Oxygen atoms give EXAFS almost identical to that from nitrogen atoms, and so the nitrogen shells of all fits to EXAFS of NH_{lt} or NH_{dk} may contain one or more oxygen atoms. NH_{lt} is, in fact, known from EPR and ENDOR studies to have one hydroxide (or possibly water) ligand.[5−7] The simplest way to reconcile these results with the crystal structures of NH_{lt} (Figure 1b) is to presume that an OH_n ligand binds to the coordination position trans to Cys110-S in the frozen solutions of NH_{lt} used for EXAFS. (The OH_n is possibly in the crystal as well, but it is unobserved in the 2.6 Å resolution structure.) Then the first coordination sphere of iron in nitrile hydratase consists of this oxygen atom, two peptide nitrogen atoms, and three cysteine sulfur atoms. However, as described before[4] and illustrated by the refined values and uncertainties of n_N in Table 1, the fits to NH_{lt} EXAFS do not prove that all three cysteine sulfur atoms remain coordinated in the frozen solution, as roughly equally good fits can be obtained assuming coordination by only two sulfur atoms.

The ambiguity between $n_S = 2$ and $n_S = 3$ is also found in our present EXAFS analyses of NH_{dk}, although for NH_{dk} (in contrast to NH_{lt}), all fitting protocols tried to give better fits with $n_S = 2$ than with $n_S = 3$. However, the relatively small difference in fit quality (compare parts c and d in Figure 4) are consistent with the possibility that all three sulfur atoms remain coordinated to the iron, as found in the crystal structure of the *Rhodococcus* sp. N-771 NH_{dk}.[13] In these crystals, two of the coordinated sulfur atoms are oxidized to sulfinate (−SO_2^-, at Cys 113) and sulfenate (−SO^-, at Cys 115) groups which help form an oxygen-rich cavity for NO binding to iron. It remains an open question as to whether the sulfur atoms are similarly bonded in the sp. R312 enzyme we are studying—the lower resolution of the crystal structure of NH_{lt} precludes confirming the existence of sulfinate and sulfenate ligands.[3] Interestingly, no evidence for sulfinic or sulfenic acid ligation was seen in resonance Raman studies of sp. R312 NH_{lt},[17] despite the strong oscillator strength of the S═O bond.

The marginal improvement of fit **V** of Table 2, or fit 21 of Table S2, relative to fit **IV** suggests a shell of several oxygen and/or carbon atoms about 3.1 Å from the iron. This shell could be due to oxygen atoms of S-ligated sulfinato or sulfenato groups; for instance, the Fe−O distances in (*S*)-(3-phenylallylsulfinato)(pentamethylcyclopentadienyl)dicarbonyliron[50] are 3.08 Å. However, just as plausible is the possibility that the ca. 3.1 Å shell is due to carbon atoms such as the C-α, C-*β*, and carbonyl carbon atoms of Cys-113, Ser-114, and/or Cys-115 (Figure 1b). Thus the EXAFS analysis neither confirms nor refutes the presence of sulfinato or sulfenato coordination to the iron in NH_{dk}.

Edge energy comparisons (Figure 2) allow us to assign the electron count of the iron in NH_{dk} as {FeNO}^{6}, i.e., with one resonance structure consisting of neutral NO bound to ferric ion. This is not surprising, given the EPR silence of NH_{dk} and

(47) Penner-Hahn, J. E.; Smith Eble, K.; McMurry, T. J.; Renner, M.; Balch, A. L.; Groves, J. T.; Dawson, J. H.; Hodgson, K. O. *J. Am. Chem. Soc.* **1986**, *108*, 7819−7825.
(48) Chance, M.; Powers, L.; Poulos, T.; Chance, M. *Biochemistry* **1986**, *25*, 1266−1270.
(49) Schappacher, M.; Weiss, R.; Montiel-Montoya, R.; Trautwein, A.; Tabard, A. *J. Am. Chem. Soc.* **1985**, *107*, 3736−3738.
(50) Churchill, M. R.; Wormald, J. *Inorg. Chem.* **1971**, *10*, 572−578.

the reports that NH_{dk} can be regenerated by reaction of the low-spin iron(III) center of NH_{lt} with 1 equiv of nitric oxide.[10,14]

The virtual identity of the EXAFS-derived Fe−N′ bond length (1.68(3) Å) and the slightly bent ∠FeN′O in NH_{dk} and **FeL(NO)**$^+$ add further support to the assignment of an {FeNO}^{6} electron count for NH_{dk}. The ∠FeN′O for both **FeL(NO)**$^+$ and NH_{dk} are determined, using a conservative method of uncertainty estimation,[30] to be within the range of 153−180° (most likely value ≈ 164°). The few extant crystal structures of {FeNO}^{6} complexes exhibit bond lengths and angles similar to the best-fit value obtained by EXAFS analysis of NH_{dk} and **FeL(NO)**$^+$. For instance, $[(OEP)Fe(NO)]^+$ has $r_{N'} = 1.64$ Å, ∠FeN′O = 177°[51] and *cis*-$((CH_3)_2NCS_2)_2(NO_2)$(NO)Fe has $r_{N'} = 1.66$ Å, ∠FeN′O = 175°.[52] Although the Fe−NO bond lengths in NH_{dk} and **FeL(NO)**$^+$ may be slightly longer than in these two {FeNO}^{6} complexes, the 1.68 ± 0.02 Å uncertainty range is also shorter than the 1.70−1.75 Å range found in crystal structures of six-coordinate {FeNO}^{7} complexes, which, with a few exceptions (for instance, angles of 167° in a diiron dinitrosyl complex[53]), have smaller ∠FeN′O values of 150 ± 10°.[53−59] Very recently, after the EXAFS analysis was complete, we were gratified to obtain a single-crystal structure of **[FeL(NO)](PF$_6$)** (Schweitzer, D.; Kovacs, J. A. Unpublished results) that shows $r_{N'} = 1.68$ Å and ∠FeN′O = 172°, with both the distance and angle within the uncertainty limits established by our analysis. The uncertainty ranges of the EXAFS-derived Fe−N′ distance and angle also encompass the values found in the crystal structure of NH_{dk} from *Rhodococcus* sp. N-771: $r_{N'} = 1.65$ Å and ∠FeN′O = 159°.[13]

On the basis of our EXAFS analysis, the average Fe−S distance is 2.27 Å for both NH_{dk} and **FeL(NO)**$^+$, which is about 0.05 Å longer than the average Fe−S distance in NH_{lt} and **FeL(N$_3$)**. Another similarity between NH_{dk} and **FeL(NO)**$^+$ is that the average Fe−N bond length (excluding the nitrosyl) is shorter by about 0.04 Å compared to the r_N determined for NH_{lt} and **FeL(N$_3$)**, respectively. Figure 4f suggests that the increased separation of the Fe−N (nonnitrosyl) and Fe−S bond distances, rather than simply the presence of the short Fe−N′ bond, is the cause of the distinct peaks at 1.5 and 1.9 Å in the FT $k^3\chi$ of both NH_{dk} and **FeL(NO)**$^+$. These changes in r_S and r_N are undoubtedly caused by electronic perturbations from the NO binding to iron. The lengthening of the average Fe−S distance in NH_{dk} can be ascribed, in part at least, to trans influence of the Fe−NO bond on the trans Fe−S(Cys110) bond. In **FeL(NO)**$^+$ the Fe−NO bond is also trans to a thiolate sulfur.

The similar changes in bond lengths induced by NO binding in nitrile hydratase and the iron complex of **L** support this ligand as a model for the protein environment of the iron in nitrile hydratase. Studies are underway to further characterize and compare the spectroscopic and reactivity properties of both nitrile hydratase and this model ligand system.

Acknowledgment. Syntheses of the iron complexes **FeL**$^+$, **FeL(N$_3$)**, and **FeL(NO)**$^+$ at UW were supported by NIH Grant 2R01GM45881. X-ray data were collected at beam line X9b, operated by the Albert Einstein Center for Synchrotron Biosciences (supported by NIH Grant RR-01633), at the National Synchrotron Light Source, Brookhaven National Laboratory, which is supported by the U.S. Department of Energy, Divisions of Materials Science and Chemical Science (DOE Contract No. DE-AC02-76CH00016).

Supporting Information Available: Tables giving amplitude and phase functions for EXAFS analysis and refined parameters from additional fits to EXAFS data and a figure showing EXAFS and FEFF simulation of **FeL(N$_3$)** (Tables S1−S6 and Figure S1) (15 pages, print/PDF). See any current masthead page for ordering information and Web access instructions.

JA973291T

(51) Scheidt, W. R.; Lee, Y. J.; Hatano, K. *J. Am. Chem. Soc.* **1984**, *106*, 3191−3198.
(52) Ileperuma, O. A.; Feltham, R. D. *Inorg. Chem.* **1977**, *16*, 1876−1883.
(53) Feig, A. L.; Bautista, M. T.; Lippard, S. J. *Inorg. Chem.* **1996**, *35*, 6892−6898.
(54) Scheidt, W. R.; Piciulo, P. L. *J. Am. Chem. Soc.* **1976**, *98*, 1913−1919.
(55) Scheidt, W. R.; Brinegar, A. C.; Ferro, E. B.; Kirner, J. F. *J. Am. Chem. Soc.* **1977**, *99*, 7315−7322.
(56) Pohl, K.; Wieghardt, K.; Nuber, B.; Weiss, J. *J. Chem. Soc., Dalton Trans.* **1987**, 187−192.
(57) Sellmann, D.; Kunstmann, H.; Moll, M.; Knoch, F. *Inorg. Chim. Acta* **1988**, *154*, 157−167.
(58) Chiou, Y.-M.; Que, L., Jr. *Inorg. Chem.* **1995**, *34*, 3270−3278.
(59) Hammes, B. S.; Ramos-Maldonado, D.; Yap, G. P. A.; Liable-Sands, L.; Rheingold, A. L.; Young, V. G., Jr.; Borovik, A. S. *Inorg. Chem.* **1997**, *36*, 3210−3211.